Metal–Organic Frameworks

International Edition: DOI: 10.1002/anie.201916201
German Edition: DOI: 10.1002/ange.201916201

Observation of Ion Electrosorption in Metal–Organic Framework Micropores with In Operando Small-Angle Neutron Scattering

Lilin He, Luming Yang, Mircea Dincă, Rui Zhang, and Jianlin Li*

Abstract: *A molecular-level understanding of transport and adsorption mechanisms of electrolyte ions in nanoporous electrodes under applied potentials is essential to control the performance of double-layer capacitors. Here, in operando small-angle neutron scattering (SANS) is used to directly detect ion movements into the nanopores of a conductive metal–organic framework (MOF) electrode under operating conditions. Neutron-scattering data reveals that most of the void space within the MOF is accessible to the solvent. Upon the addition of the electrolyte sodium triflate (NaOTf), the ions are adsorbed on the outer surface of the protrusions to form a 30 Å layer instead of entering the ionophobic pores in the absence of an applied charging potential. The changes in scattering intensity when potentials are applied suggests the ion rearrangement in the micropores following different mechanisms depending on the electrode polarization. These observations shed insights on ion electrosorption in electrode materials.*

Introduction

Supercapacitors (SCs) or electrical double-layer capacitors (EDLCs) are a key element in the energy-storage landscape, especially towards vehicle electrification.[1] The fast electrosorption of ions inside the pores of the porous electrodes under an applied external voltage endows SCs significantly higher power density and longer lifetime than batteries where slow faradaic reactions or limited ion-intercalation take place.[2] The applications of SCs have been broadened from past mundane applications into numerous industrial and consumer applications.[3] Despite their advantages of high specific power, high energy efficiency, practically unlimited cycle life, SCs suffer from much lower energy density, particularly in comparison with Li-ion batteries. Improving SCs has led to a two-pronged approach: the development of new electrode materials and electrolytes as well as designing/optimizing the morphology and porosity of existing electrode materials. Both depend critically on a deep understanding of the energy storage mechanisms,[4] including an understanding of the relationship between the pore size and accessible surface area.[2,5–7] It is traditionally believed that the pores should be substantially larger than the size of solvated electrolyte ions to allow the ions to diffuse into the nanopores to achieve high capacitance. However, experimental studies found that subnanometer pores could maximize the capacitance of carbide-derived carbon (CDC) materials and subsequent theoretical calculations and molecular simulations verified the anomalous phenomenon.[8–10] The anomaly was originally ascribed to the distorted solvation or partial desolvation of counterions that lead to a closer distance between the ion center and electrode surface.[8] It was later observed that the maximized capacitance could be achieved when the ion size matched the pore size using solvent-free ionic liquids (ILs).[11] Huang et al. proposed a wire-in-cylinder model to take into account the effects of pore curvature on the capacitance of nanoporous carbons, which explained the observed anomalous increase in capacitance for pores below 1 nm.[10] Using molecular dynamics simulations (MD) and classical density functional theory (DFT), Feng and Jiang separately revealed that the capacitance exhibited an oscillatory mode as the pore width varied. The capacitance versus pore size was found to exhibit a strong peak for subnanometer pores.[12] Experimental data are required to verify and validate these computer simulations.

The last decade has also witnessed the rapid development of a few in situ characterization techniques to advance the understanding of charge storage mechanism in the carbon-based supercapacitors. Among them are nuclear magnetic resonance (NMR), infrared spectroscopy (IR), electrochemical quartz crystal microbalance (EQCM), and small angle X-ray and neutron scattering (SAXS, SANS respectively).[13–16] SAXS and SANS are capable of noninvasively and non-destructively studying the pore-size dependence of pore wettability and ion electrosorption based on the changes of contrast between the pore space and the pore wall while ions are injected and ejected from the pores under applied potentials. These scattering techniques combined with computer simulations have been used to quantify changes in the populations of adsorbed species during charging and provided

[*] Dr. L. He
Neutron Scattering Division, Oak Ridge National Laboratory
Oak Ridge, TN 37831 (USA)
E-mail: hel3@ornl.gov
L. Yang, Prof. M. Dincă
Department of Chemistry, Massachusetts Institute of Technology
77 Massachusetts Avenue, Cambridge, MA 02139 (USA)
Dr. R. Zhang
Energy and Mineral Engineering, Penn State University
University Park, PA 16802 (USA)
Dr. J. Li
Energy & Transportation Science Division
Oak Ridge National Laboratory
Oak Ridge, TN 37831 (USA)

Supporting information (material characterization: static SANS, powder X-ray diffraction, electrode preparation, in operando SANS techniques; experimental details: SANS data analysis, neutron scattering length densities, incoherent scattering cross-sections of chemical species) and the ORCID identification number(s) for the author(s) of this article can be found under: https://doi.org/10.1002/anie.201916201.

novel insights into ion transport and charge storage mechanisms within carbon nanopores.[16]

Although considerable progress has been made by the development of advanced experimental methods and computer simulations, there are still on-going debates on the charge storage mechanisms in carbon-based electrodes due to the complexity of charging process in supercapacitors.[5,17] As proposed by Forse and co-workers based on experimental observations and computer simulations, many factors, i.e., electrode polarization, voltage, electrolyte ion size and symmetry, electrode materials, pore architecture may have a synergistic impact on the charging processes.[5] In previous reports, mesoporous carbonaceous nanomaterials have been exclusively selected as model electrode materials owning to their good electrical conductivity, tunable pore architecture and functionable surface.[17] However, important but often ignored fact in all of these studies is that carbon electrodes were assumed to have identical slit shape in order to obtain pore-size distribution using gas adsorption and DFT methods, which is definitely problematic.[7,17] Real carbon materials exhibit very complex features, that is, various shapes, size distribution and different accessibility with each size range. The lack of long-range order makes the characterization of charge storage at the molecular level rather challenging. Therefore, nanoporous materials with uniform shape, narrow distribution pores are desirable for mechanism studies.[12]

Metal–organic frameworks (MOFs), a class of porous crystalline materials, consist of metal ions or clusters coordinated to organic ligands. They have generated a tremendous amount of interest in widespread areas ranging from electrochemical energy storage, gas storage and separation, catalyst immobilization to water desalination, owing to their ultrahigh porosity, well-defined and tailorable pore architectures, and functionalizable surface.[18] The high porosity of most MOF materials, however, is inherently coupled with very poor electrical conductivity, which limits their applications as electrodes in EDLCs. Recently Sheberla et al. developed a conductive porous MOF, $Ni_3(HITP)_2$ (HITP = 2,3,6,7,10,11-hexaiminotriphenylene) with an excellent electronic conductivity.[19] The material is composed of stacked π-conjugated two-dimensional layers, penetrated by one-dimensional cylindrical channels of about 15 Å diameter. It showed a loss of only 10% in capacitance and no increase in the ESR after 10000 cycles. The surface area of the MOF was 630 $m^2 g^{-1}$, as determined through N_2 adsorption isotherm based on the Brunauer–Emmett–Teller (BET) theory. More interestingly, the material could serve as free-standing electrodes without additives or other binder after pressed into self-supported pellets at high pressure, which makes it an ideal material to study the ion electrosorption in micropores during the charging process.[19,20]

Herein, we report insights into ion arrangements within the conductive $Ni_3(HITP)_2$ MOF electrode using in operando SANS. The method provides not only direct and accurate information on the multi-length scale morphology of dry MOF and pore accessibility upon soaked with solvent, but also the changes of species confined in the micropores with and without applied potential. This study reveals that the charge storage strongly depends on the polarization of electrode. The findings observed in this work would greatly advance our understanding of the charge storage mechanisms under nanoconfinement.

Results and Discussion

All of the SANS measurements in this work were carried out on the general-purpose SANS instrument (GP-SANS) at the High Flux Research reactor (HFIR), Oak Ridge National Laboratory. The detailed experimental description can be found in the Supporting Information.

Morphology of the Dry MOF

A radially symmetrical 2D SANS pattern is observed for the pristine MOF sample. The raw data is azimuthally averaged to get 1D curve, which is shown in a log–log graph in Figure 1a. The curve exhibits three main regimes, arising from different levels of hierarchy of the MOF structure. In the low q region of 0.007–0.06 $Å^{-1}$, the intensity decays following power law q^{-D} with an exponent D between 2 and 3, suggesting the mass fractal that arises from the open mass network structure resulted from the aggregation of the pores as the monomer.[21,22] This structural feature is different than the surface fractal features frequently observed in most porous carbons.[23,24] A broad shoulder at about 0.06 $Å^{-1}$ makes it transition from mass fractal to Porod scattering regime. A nearly q^{-4} decay of scattering intensity in the q range of 0.06–0.15 $Å^{-1}$ indicates relatively sharp and smooth solid matrix-pore interfaces, which allows the model-independent evaluation of the specific surface area (SSA) based on the Porod law.[25] The calculated SSA from the scattering curve is about 871.7 $m^2 g^{-1}$ considering a skeletal density of 1.1 ± 0.2 $g cm^{-3}$. This value is higher than the reported Brunauer–Emmett–Teller (BET) value of 630 $m^2 g^{-1}$.[19] The discrepancy arises from two facts. One is that neutron scattering detects all the pores including open pores and close pores that probing gas molecules have no access to. The other fact is that both methods have different cutoffs of pore size to probe.[26] The crossover from a mass fractal to a surface scattering occurs at the scattering moment corresponding to the reciprocal of the size of populated objects. In the high q regime, a sharp peak located at about 0.35 $Å^{-1}$ represents the crystalline ordering of cylindrical pores, which gives the center-to-center distance and agrees reasonably well with the pore size measured from N_2 adsorption isotherm.[19] The fitting of full curve using a summed model of fractal cylinder and a Lorentzian function indicates that the object giving rise to the scattering shoulder is about 163.7 Å in length and about 50.0 Å in diameter (see the fitting model described in the Supporting Information). These dimensions reflect the average size of meso-sized leaf-like protrusions that contain ordered micropores (see SEM image in Figure 1b).

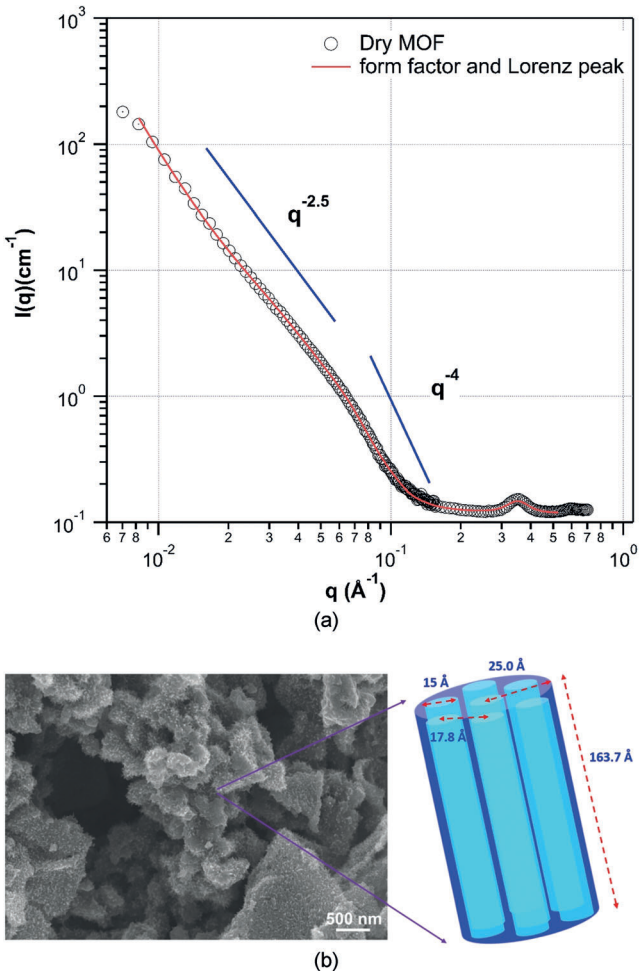

Figure 1. a) Double logarithmic representation of the scattering intensity $I(q)$ of the MOF electrode under dry conditions. The solid red line corresponds to the best fit using the summed model (explained in detail in the Supporting Information, Methods). b) SEM image and sketch of the cylindrical protrusion. The dimensions of arranged pores were obtained based on the model fitting. The length and the radius of the leaf-like protrusions are 163.7 Å and 25 Å, respectively. The center-to-center distance between the micropores is 17.8 Å. The pore size of 15 Å was obtained from the gas adsorption method.

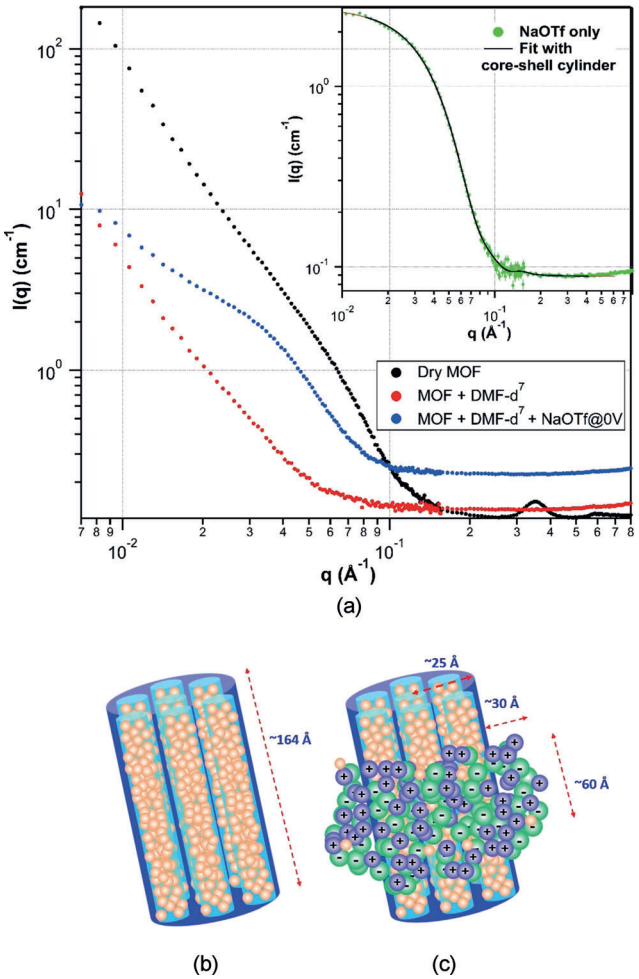

Figure 2. a) SANS profiles of dry MOF (black), MOF with deuterated DMF (red) and MOF with electrolyte in solution (green). The inset shows the net scattering contributed by NaOTf. The solid black line in the inset corresponds to the model fitting using the core–shell cylinder form. b) Illustration of the MOF pores filled with solvent molecules at 0 V. c) Ion aggregate around the protrusions to form a layer with 60 Å in length and 30 Å in thickness at 0 V. Yellow: solvent molecules, purple: Na^+, green: OTf^-.

Solvent Penetration in the MOF

Upon the addition of deuterated dimethylformamide (DMF), the peak at 0.353 $Å^{-1}$ vanishes, indicating that the majority of the micropores are accessible to the solvent molecules (Figure 2). Solvent wetting of carbon electrodes at the null potential has been observed in simulations.[7] The scattering in the low q region dramatically drops owing to the penetration of solvent into the interstitial spaces between the protrusions and between granular particles. The scattering intensity is proportional to the contrast between the pore space and the solid matrix within the two-phase approximation:

$$I(q) \propto (\rho_{MOF} - \rho_{SPACE})^2 \quad (1)$$

where ρ_{MOF} and ρ_{SPACE} are neutron scattering length density (NSLD) of the MOF and the space, respectively. Assuming all these spaces are accessible to the solvent, a 98-fold drop, or about 99 % in percentage, in scattering intensity is expected in terms of:

$$\frac{I_{EMPTY}(q)}{I_{FILLED}(q)} = \frac{(5.753-0)^2}{(6.334-5.753)^2} = 98 \quad (2)$$

However, the actual decrease of the scattering intensity at $q = 0.008$ $Å^{-1}$ is about 95% instead of 99%, which is attributed to the pores that are inaccessible to the solvent. It is worth noting that broad shoulder near 0.06 $Å^{-1}$ also disappears due to the decreasing scattering contrast between two phases in the sample. The MOF maintains its original crystallinity structure upon exposure to the solvent, which can be seen from the SANS graph of hydrogenated DMF (Supporting Information, Figure S2). The background level slightly increases owing to the incoherent scattering of the solvent.

Ion Packing at Zero Applied Potential

On the SANS curve of the MOF electrode, a broad shoulder at about 0.04 $Å^{-1}$ develops when the electrode is soaked with a solution of 1 mol L^{-1} NaOTf in deuterated DMF in the absence of an electric field (Figure 2a). NaOTf is chosen in this work owing to the significantly different NSLDs and incoherent scattering cross-sections of the cation and the anion (see NSLDs in the Supporting Information, Table S1). The addition of Na^+ leads to an increase in incoherent scattering background (see the incoherent scattering cross sections of different species in the Supporting Information, Table S1). The net scattering signal contributed by the adsorbed cations and anions can be obtained after the subtraction of the scattering contributions of MOF and the solvent, as shown in the inset of Figure 2a, where the solid line corresponds to a core–shell cylinder model fitting. The fitting parameters are summarized in Table 1. The radius of about 55 Å for the cylinder is more than twice as large as that of the dry MOF, suggesting a large number of ions are adsorbed on the outer surface of the protrusions at the null potential to form a circa 30 Å layer (see illustration in Figure 2c). However, the ionic aggregates are about 60 Å in length, significantly shorter than the protrusions (ca. 164 Å). This could be attributed to the fact that ion density near the end of each protrusion gradually decays to the bulk ion density in solution (see the illustration in Figure 2c). The core region shows a significantly lower NSLD than that of the shell region, which can be ascribed to the hydrogen atoms in the MOF.

Ion Rearrangement under Applied Potentials

To investigate changes in the ion behavior under operating conditions, in operando SANS measurements were performed as the cell was sequentially charged with voltages from 0 to +0.1 V, −0.4 V, +0.3 V. The experimental setup is shown in the Supporting Information, Figure S2. The SANS profiles at these potentials are displayed in Figure 3a. At each potential, the data collection started at full equilibration. At +0.1 V, OTf^- ions enter the pores via the counter-ion adsorption mechanism, resulting in a reduced NSLD in the core region of the core–shell cylinder, which is obtained through the model fitting using a core–shell cylinder form factor (Table 1). Both the length of the cylinder and the core radius significantly increase, whereas the shell thickness changes minimally at this potential. When the electrode is subsequently biased at −0.4 V, a decrease in the cylinder length and the core radius takes place, with retention of the overall shell dimension. Interestingly, the NSLD of the core

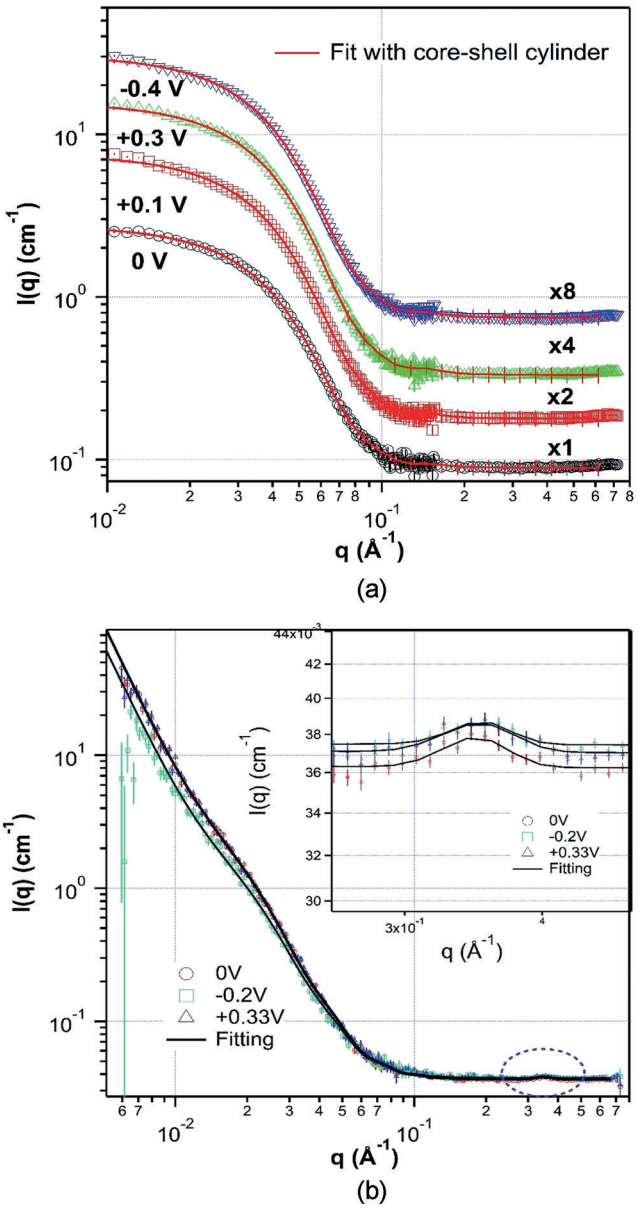

Figure 3. a) Double logarithmic representation of MOF with electrolyte in solution at various potentials. The data are vertically shifted for visibility. The solid line in each curve corresponds to the model fitting using the cylinder form. b) SANS profiles of the MOF electrode under three voltages. The solid line represents the fitting using a summed model with a mass fractal cylinder and a Lorentzian function. The inset plot highlights the change of peak at 0.353 $Å^{-1}$.

Table 1: Fitting parameters of SANS profiles under various potentials using a core–shell cylinder form.

Potential [V]	Core radius [Å]	Shell radius [Å]	Cylinder length [Å]	Core NSLD [$\times 10^{-6}$ $Å^{-2}$]	Shell NSLD [$\times 10^{-6}$ $Å^{-2}$]	I_{inc} [cm^{-1}]
0	24.93 ± 0.45	29.58 ± 0.22	60.44 ± 1.68	4.69 ± 0.02	6.07 ± 0.01	0.0889 ± 0.0001
+0.1	26.45 ± 0.36	29.96 ± 0.19	64.12 ± 1.42	4.54 ± 0.02	6.05 ± 0.01	0.0890 ± 0.0001
−0.4	25.06 ± 0.29	30.45 ± 0.14	61.68 ± 1.07	4.44 ± 0.02	6.03 ± 0.01	0.0931 ± 0.0001
+0.3	25.13 ± 0.40	29.78 ± 0.21	62.87 ± 1.53	4.47 ± 0.02	6.02 ± 0.01	0.0824 ± 0.0002

further declines from that observed at +0.1 V. The expected behavior would be an increase of the core NSLD if Na^+ ions enter the pores following pure ion swapping mechanism because of the larger NSLD of Na^+ than that of OTF^-. Presumably, the expulsion of $[D_7]$DMF out of the pores by Na^+ ions also takes place simultaneously with the ion exchange process. Moreover, this process must be dominated to overcome the effect of increasing number of Na^+ in the pores for accounting for the eventual decreased core NSLD (Table 1). The switch of charging voltage from −0.4 V to +0.3 V results in increased length of the ionic cylinder and core radius as anticipated. The noticeable increase in core NSLD under this potential indicates that solvent molecules move into the pores to replace Na^+ ions through co-ion desorption mechanism. If the ion exchange mechanism takes places simultaneously with the co-ion desorption mechanism, the co-ion desorption has to be dominant to account for the subtle increase of the core NSLD. The majority of OTf^- ions are adsorbed on the outer surface of the protrusions to balance the charge of the electrode, which is evidenced by the decreased NSLD of the shell (Table 1). The incoherent scattering background is another indicator for the movements of ions under the charging process. Na^+ possesses a higher incoherent scattering cross section than OTf^-. Thus, negative potential results in an appreciably higher incoherent scattering background.

SANS also allows exploring the species inside the micropores by observing changes of neutron scattering intensity of the 0.353 $Å^{-1}$ peak during charging. Indeed, owing to the large contrast between OTF^- and the MOF wall, we would expect the correlation peak at 0.353 $Å^{-1}$ to reappear upon applying a +0.1 V bias if OTf^- ions enter the pores through a pure counter-ion adsorption mechanism. However, this peak was not observed, which suggests that considerable pore space was still occupied by the DMF molecules at this potential. Presumably, large OTF^- ions must overcome both an entropic barrier to enter the relatively narrow pores, and an electrostatic barrier from neighboring ions, which is energetically unfavorable. The recurrence of the correlation peak was not observed owing to the subtle change of the NSLD in the micropores.

To further investigate the changes of species inside the micropores, we subsequently employed a coin cell setup (Supporting Information, Figure S3) to monitor ion movements in the micropores during the charging process. In these measurements, we used hydrogenated DMF instead of deuterated DMF by taking advantage of the isotope sensitivity of neutrons. The thin sample inside of coin-cell (ca. 1 mm) allows for the use of h-DMF by minimizing multiple scattering and incoherent scattering from the hydrogens in the solvent. The height and width of the peak located at 0.353 $Å^{-1}$ are sensitive to the organization of electrolyte and solvent molecules inside the micropores. Figure 3b displays the SANS profiles upon changing the potential. A Lorentzian model was used to fit the peak and the fitting parameters are listed in Table 2.

Table 2: Changes in micropores under potentials.

Potential [V]	Peak height [$\times 10^{-3}$]	Peak position [$Å^{-1}$]	FWHM
0	1.59 ± 0.19	0.348 ± 0.003	0.023 ± 0.003
−0.20	1.26 ± 0.22	0.352 ± 0.004	0.022 ± 0.004
+0.33	1.57 ± 0.21	0.351 ± 0.004	0.026 ± 0.004

When charging the electrode under −0.20 V, a drop in peak height from 1.59 to 1.26 indicate that Na^+ ions enter the micropores via counter-ion adsorption mechanism, which decreases the contrast between the pore and the solid wall. Under the positive potential of +0.33 V, on the contrary, Na^+ ions in the micropores leave the pores following combined

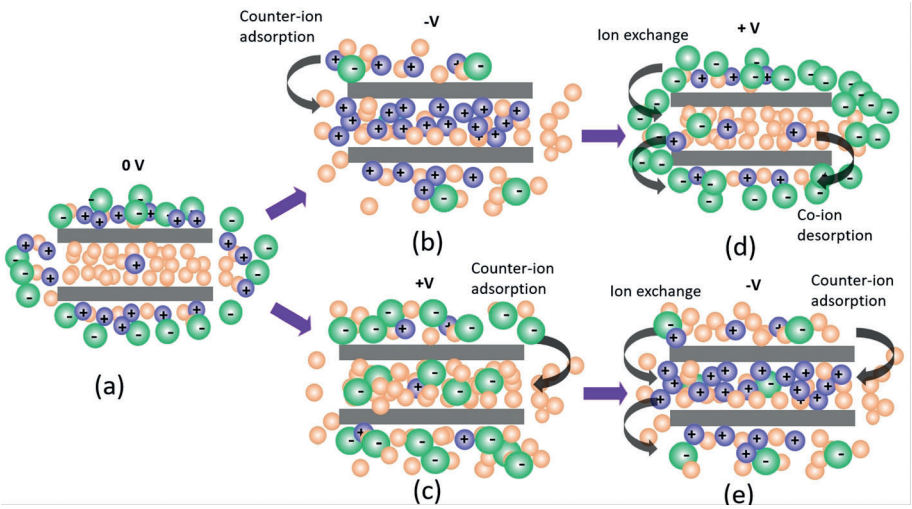

Figure 4. Different charging mechanisms for ionophobic MOF micropores depending on the polarization of the electrode. Yellow solvent molecules, purple Na^+, green OTF^-. a) At 0 V, the ionophobic pores are filled with solvent molecules. b),c) From 0 V to a negative potential or positive potential, the charging goes majorly through counter-ion adsorption. d) Switch the potential from negative to positive, co-ion (Na^+) desorption dominates, ion exchange mechanism may take place simultaneously. e) Switch the potential from positive to negative, counter-ion (Na^+) adsorption dominates, ion exchange mechanism could occur simultaneously.

mechanisms of ion exchange and co-ion desorption, which results in a larger contrast between the pore and the wall. Therefore, an increase in the peak height is observed in comparison with that at the negative polarization (Table 2). This is consistent with our previous observations. The different charging mechanisms at different polarization conditions are illustrated in Figure 4.

If the micropores are ionophilic and Na^+ ions are present in the pores at the null potential, we should anticipate a greater peak height at +0.33 V compared with that at 0 V once most of these initial Na^+ ions leave the pores. However, the peak heights at 0 V and at +0.33 V are comparable (Table 2), which suggests that the micropores have only negligible amount of Na^+ ions at 0 V. Kondrat et al. have described two kinds of pores in porous electrodes, ionophilic and ionophobic, in their simulation. Their results showed that electrodes with ionophobic pores could facilitate fast charging and suggested that the energy capacity is higher for materials with ionophobic pores.[27,28] This is the first time, to the best of our knowledge, that ionophobic pores have been experimentally observed. The center-to-center distance between the micropores, reflected by the peak position, indicates no noticeable expansion of the pores. The peak broadening, coming from both lattice imperfection and instrument resolution and indicated by full-width at half-maximum (FWHM), shows negligible change revealing that the material retains its ordered arrangement during charging process.

Conclusion

We have used in operando SANS to probe ion electrosorption into a conductive MOF. The dry MOF is composed of cylindrical protrusions with embedded micropores. Most of the space within the MOF including micropores and interstitial volume are accessible to the solvent. Electrolyte ions are adsorbed on the outer surface of the protrusions instead of entering the micropores at null potential. Our results also indicate that the ionophobicity of the micropores causes pure counter-ion adsorption when applying a nonzero bias voltage. Subsequent charging process exhibits different storage mechanisms strongly depending on the polarization of electrode. When switching from negative to positive polarization the process proceeds predominantly through the co-ion desorption mechanism, whereas switching from a positive to a negative polarization, the charging process majorly follows the counter-ion adsorption mechanism. These results provide molecular level insight into the charging mechanisms in the MOF electrode.

Acknowledgements

This research used resources at the High Flux Isotope Reactor, DOE Office of Science User Facilities operated by the Oak Ridge National Laboratory. Research sponsored by the Laboratory Directed Research and Development Program of Oak Ridge National Laboratory, managed by UT-Battelle, LLC, for the U.S. Department of Energy.

Conflict of interest

The authors declare no conflict of interest.

Keywords: electrosorption · metal–organic frameworks · microporous materials · small-angle neutron scattering · supercapacitors

[1] F. Béguin, F. V. Presser, A. Balducci, E. Frackowiak, *Adv. Mater.* **2014**, *26*, 2219 – 2251.
[2] M. Salanne, B. Rotenberg, K. Naoi, K. Kaneko, P. L. Taberna, C. P. Grey, B. Dunn, P. Simon, *Nat. Energy* **2016**, *1*, 16070.
[3] Y. G. Wang, Y. F. Song, Y. Y. Xia, *Chem. Soc. Rev.* **2016**, *45*, 5925 – 5950.
[4] G. P. Wang, L. Zhang, J. J. Zhang, *Chem. Soc. Rev.* **2012**, *41*, 797 – 828.
[5] A. C. Forse, C. Merlet, J. M. Griffin, C. P. Grey, *J. Am. Chem. Soc.* **2016**, *138*, 5731 – 5744.
[6] F. X. Wang, X. W. Wu, X. H. Yuan, Z. C. Liu, Y. Zhang, L. J. Fu, Y. S. Zhu, Q. M. Zhou, Y. P. Wu, W. Huang, *Chem. Soc. Rev.* **2017**, *46*, 6816 – 6854; A. Karatrantos, Q. Cai, *Phys. Chem. Chem. Phys.* **2016**, *18*, 30761 – 30769.
[7] C. Zhan, C. Lian, Y. Zhang, M. W. Thompson, Y. Xie, J. Z. Wu, P. R. C. Kent, P. T. Cummings, D. E. Jiang, D. J. Wesolowski, *Adv. Sci.* **2017**, *4*, 1700059.
[8] J. Chmiola, G. Yushin, Y. Gogotsi, C. Portet, P. Simon, P. L. Taberna, *Science* **2006**, *313*, 1760 – 1763.
[9] P. Simon, Y. Gogotsi, *Philos. Trans. R. Soc. London Ser. A* **2010**, *368*, 3457 – 3467; X. H. Wang, A. Y. Mehandzhiyski, B. Arstad, K. L. Van Aken, T. S. Mathis, A. Gallegos, Z. Q. Tian, D. D. Ren, E. Sheridan, B. A. Grimes, D. E. Jiang, J. Z. Wu, Y. Gogotsi, D. Chen, *J. Am. Chem. Soc.* **2017**, *139*, 18681 – 18687.
[10] J. S. Huang, B. G. Sumpter, V. Meunier, *Angew. Chem. Int. Ed.* **2008**, *47*, 520 – 524; *Angew. Chem.* **2008**, *120*, 530 – 534.
[11] C. Largeot, C. Portet, J. Chmiola, P. L. Taberna, Y. Gogotsi, P. Simon, *J. Am. Chem. Soc.* **2008**, *130*, 2730 – 2731.
[12] G. Feng, P. T. Cummings, *J. Phys. Chem. Lett.* **2011**, *2*, 2859 – 2864; D. E. Jiang, Z. H. Jin, J. Z. Wu, *Nano. Lett.* **2011**, *11*, 5373 – 5377.
[13] M. Deschamps, E. Gilbert, P. Azais, E. Raymundo-Pinero, M. R. Ammar, P. Simon, D. Massiot, F. Beguin, *Nat. Mater.* **2013**, *12*, 351 – 358; H. Wang, T. K. J. Koster, N. M. Trease, J. Segalini, P. L. Taberna, P. Simon, Y. Gogotsi, C. P. Grey, *J. Am. Chem. Soc.* **2011**, *133*, 19270 – 19273.
[14] F. W. Richey, B. Dyatkin, Y. Gogotsi, Y. A. Elabd, *J. Am. Chem. Soc.* **2013**, *135*, 12818 – 12826.
[15] M. D. Levi, G. Salitra, N. Levy, D. Aurbach, J. Maier, *Nat. Mater.* **2009**, *8*, 872 – 875.
[16] S. Boukhalfa, L. L. He, Y. B. Melnichenko, G. Yushin, *Angew. Chem. Int. Ed.* **2013**, *52*, 4618 – 4622; *Angew. Chem.* **2013**, *125*, 4716 – 4720; C. Prehal, D. Weingarth, E. Perre, R. T. Lechner, H. Amenitsch, O. Paris, V. Presser, *Energy Environ. Sci.* **2015**, *8*, 1725 – 1735.
[17] A. García-Gómez, G. Moreno-Fernández, B. Lobato, T. A. Centeno, *Phys. Chem. Chem. Phys.* **2015**, *17*, 15687 – 15690; T. A. Centeno, O. Sereda, F. Stoeckli, *Phys. Chem. Chem. Phys.* **2011**, *13*, 12403 – 12406; A. Eftekhari, *Mater. Today Chem.* **2018**, *7*, 1 – 4.
[18] H. B. Wu, X. W. Lou, *Sci. Adv.* **2017**, *3*, eaap9252; G. Y. Xu, P. Nie, H. Dou, B. Ding, L. Y. Li, X. G. Zhang, *Mater. Today* **2017**, *20*, 191 – 209; H. Furukawa, K. E. Cordova, M. O'Keeffe, O. M. Yaghi, *Science* **2013**, *341*, 1230444.

[19] D. Sheberla, J. C. Bachman, J. S. Elias, C. J. Sun, Y. Shao-Horn, M. Dincă, *Nat. Mater.* **2017**, *16*, 220 – 224; S. Bi, H. Banda, M. Chen, L. Niu, M. Chen, T. Wu, J. Wang, R. Wang, J. Feng, T. Chen, M. Dincă, A. A. Kornyshev, G. Feng, *Nat. Mater.* **2020**, https://doi.org/10.1038/s41563-019-0598-7.
[20] D. Sheberla, L. Sun, M. A. Blood-Forsythe, C. R. Wade, Er, C. K. Brozek, A. Aspuru-Guzik, M. Dincă, *J. Am. Chem. Soc.* **2014**, *136*, 8859 – 8862.
[21] P. McMahon, I. Snook, *J. Chem. Phys.* **1996**, *105*, 2223 – 2227.
[22] D. F. R. Mildner, P. L. Hall, *J. Phys. D* **1986**, *19*, 1535 – 1545.
[23] H. D. Bale, P. W. Schmidt, *Phys. Rev. Lett.* **1984**, *53*, 596 – 599.
[24] L. L. He, Y. B. Melnichenko, N. C. Gallego, C. I. Contescu, J. J. Guo, J. Bahadur, *Carbon* **2014**, *80*, 82 – 90.
[25] O. Glatter, O. Kratky, *Small angle x-ray scattering*, Academic Press, London, **1982**.
[26] L. M. Anovitz, D. R. Cole, *Rev. Mineral. Geochem.* **2015**, *80*, 61 – 164.
[27] S. Kondrat, P. Wu, R. Qiao, A. A. Kornyshev, *Nat. Mater.* **2014**, *13*, 387 – 393.
[28] S. Kondrat, A. A. Kornyshev, *Nanoscale Horiz.* **2016**, *1*, 45 – 52.

Manuscript received: December 17, 2019
Revised manuscript received: March 9, 2020
Accepted manuscript online: March 11, 2020
Version of record online: ■■ ■■, ■■■■

Research Articles

Metal–Organic Frameworks

L. He,* L. Yang, M. Dincă, R. Zhang, J. Li ——— ■■■■–■■■■

Observation of Ion Electrosorption in Metal–Organic Framework Micropores with In Operando Small-Angle Neutron Scattering

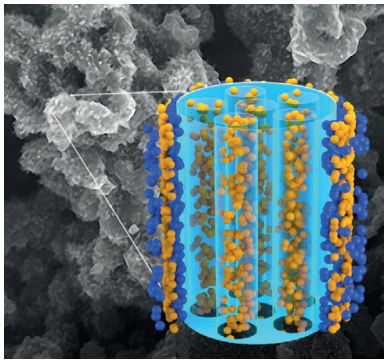

Ion arrangements in a conductive MOF electrode are examined with in operando neutron scattering. The non-destructive method provides direct and accurate information on the multi-length scale morphology of the dry MOF, the pore accessibility upon soaking with solvent and electrolyte, and the changes in species confined within the micropores under operating conditions.